Stable Interaction Of The UK B.1.1.7 lineage SARS-CoV-2 S1 Spike N501Y Mutant With ACE2 Revealed By Molecular Dynamics Simulation

Wesam Ahmed[1], Angelin M Philip[1], Kabir H Biswas[1,*]

Affiliation:

[1]College of Health & Life Sciences, Hamad Bin Khalifa University, Qatar Foundation, Doha – 34110, Qatar

***Correspondence:** kbiswas@hbku.edu.qa

Keywords: ACE2; COVID-19; Molecular Dynamics Simulation; SARS-CoV-2; S1 Spike Protein; N501Y mutant;

Abstract

COVID-19 caused by SARS-CoV-2 has caused a massive health crisis across the world, and genetic variants such as the D614G gaining enhanced infectivity and competitive fitness have significantly aggravated the global concern. In this regard, the latest SARS-CoV-2 variant, B.1.1.7 lineage, reported from the United Kingdom (UK) is of great significance, in that it contains several mutations that increases its infection and transmission rates as evidenced by the increased number of clinical reports. Specifically, the N501Y mutation in the SARS-CoV-2 S1 receptor binding domain (RBD) domain has been shown to possess increased affinity for ACE2, although the basis for this not yet clear. Here, we dissect the mechanism underlying the increased affinity using molecular dynamics (MD) simulations of the available ACE2-S1-RBD complex structure (6M0J) and show a prolonged and stable interaction of the Y501 residue in the N501Y mutant S1-RBD with interfacial residues, Y41 and K353, in ACE2 as compared to the wild type S1-RBD. Additionally, we find that the N501Y mutant S1-RBD displays altered dynamics that likely aids in its enhanced interaction with ACE2. By elucidating a mechanistic basis for the increased affinity of the N501Y mutation in S1-RBD for ACE2, we believe that the results presented here will aid in developing therapeutic strategies against SARS-CoV-2 including designing drugs targeting the ACE2-S1-RBD interaction.

Introduction

Severe acute respiratory syndrome coronavirus 2 (SARS-CoV-2) is a positive-sense, single stranded, enveloped RNA virus that belongs to the *Coronaviridae* family and is the causative agent of the COVID-19 pandemic.[1, 2] As of December 2020, more than 80 million cases have been reported worldwide, with more than 1.7 million deaths (https://covid19.who.int/). In general, the coronaviruses express four structural protein: nucleocapsid (N) protein that encapsulate the genomic material, membrane (M) and envelope (E) proteins, both of which ensure encapsulation of the viral genome, and the envelope-anchored spike (S) protein that protrudes from the viral surface and facilitates viral attachment and entry into host cells. The latter is made up of two subunits, namely S1 and S2. Viral attachment to host cells occurs through binding of its S1 subunit – also known as the receptor binding domain (RBD) – to the host cell membrane-localized angiotensin converting enzyme 2 (ACE2) receptor, which catalyzes the hydrolysis of angiotensin II, a vasoconstrictor, to the heptapeptide angiotensin-(1-7), a vasodilator.[3] It is important to note that the affinity of S1-RBD of SARS-CoV-2 for ACE2 was reported to be 10 times higher than that of SARS-CoV-1, providing a biochemical basis for the increased infection efficiency of SARS-CoV-2 compared to SAR-CoV-1. Indeed, the ACE2-S1-RBD interaction has become an attractive target for inhibiting viral entry into the host cell.[4-8] For instance, the human recombinant soluble ACE2 protein has been utilized for reducing SARS-CoV-2 binding to the cellular ACE2 receptor leading to reduced injury to multiple organs, including the lungs, kidneys, and heart.[9] Similarly, monoclonal antibodies such as 18F3 and 7B11 have been developed to neutralize SARS-CoV-2 infection by blocking epitopes on the S1-RBD.[10]

On top of the increased affinity of SARS-CoV-2 S1-RBD to ACE2 compared to SARS-CoV-1, new genetic variants with increased infectivity and virulence, likely arising under increased immunological pressure in patients suffering from COVID-19 or convalescent plasma therapy [11, 12], have further complicated our efforts towards thwarting the pandemic. One of the key examples of such variants is the S1-RBD D614G mutant that has outcompeted the Wuhan-Hu-1 or the ancestral SARS-CoV-2 strain.[13-16] A comparative study conducted by Hou *et al* observed that this variant is superior in infecting the epithelial cells and replicates in higher number than the ancestral virus. The structural analysis showed that the S1-RBD containing the D614G mutation are more flexible and explore the open conformation more than the wild type protein, thus, leading to an increased affinity for ACE2.[14, 17, 18]

In the recent times, a new phylogenetic group of SARS-CoV-2 (lineage B.1.1.7) has been identified in the COVID-19 Genomics UK Consortium dataset with greater than 50% of the cases belonging to this new cluster B.1.1.7 lineage that has an estimated about 50 to 70% increased transmissibility, as per epidemiological and virological investigations.[19, 20] Indeed, reports of the presence of this variant has emerged from other countries as well. Sequence analysis indicates the presence of a total of 17 mutations spanning the ORF1ab, spike, Orf8 and the N protein in the genome of this variant**.**[20] Majority of these mutations (8 out of the total 17), however, are present in the spike protein. These include deletions mutations ΔH69V70 and ΔY144 and missense mutations N501Y, A507D, P681H, T716I, S982A and D1118H. Of these, the N501Y missense mutation strikes out as one of the most interesting ones due to its presence at the ACE2-S1-RBD interaction interface [21] raising the possibility of an altered interaction between the two proteins. In fact, deep mutational analysis of S1-RBD, in combination with the

yeast-surface-display platform, has revealed an increased affinity of the N501Y mutant S1-RBD to ACE2 (apparent K_d of 3.9×10^{-11} M for the wild type vs. 4.9×10^{-11} M for the N501Y mutant).[22]

In the current study, we performed multiple all atom, explicit solvent MD simulations to gain an insight into the mechanism underlying the increased affinity of the N501Y mutant S1-RBD for ACE2. Simulations of the wild type and the N501Y mutant S1-RBD in complex with ACE2 revealed an overall decreased dynamics in the mutant as compared to the wild type complex. Importantly, these simulations showed a prolonged and stable interaction between the Y501 residue with the neighbouring Y41 and K353 residues in ACE2 in the mutant complex as compared to the N501 residue in the wild type complex.

Materials & Methods

ACE2-S1-RBD structure preparation

The three-dimensional structure of the ACE2-S1-RBD complex spanning residues S19 to D614 of ACE2 and R319 to G526 of S1-RBD was obtained from the RCSB PDB website as a PDB file (PDB ID: 6M0J).[21] PyMOL (The PyMOL Molecular Graphics System, Version 2.0.0, Schrödinger, LLC; pymol.org) was used to visualize the three-dimensional structure and to generate the N501Y mutant structure using the Mutagenesis tool plugin available in PyMOL. PDB files were saved after removing ions, solvent, and water molecules.

ACE2-S1-RBD molecular dynamics simulations

Molecular dynamics simulations were performed using the NAMD2-14 software.[23] The simulation system consisting of the molecular complex formed by the ACE2-S1-RBD was prepared using the QwikMD Toolkit [24] available as a part of the Visual Molecular Dynamics (VMD) software [25]. Specifically, the protein complex was simulated in an explicit aqueous solvent containing 0.15 M NaCl concentration and at a temperature of 310 K (with a total of about 450000 atoms). Molecular dynamics simulations were performed using the default parameters including a 2-fs time-step, a pressure of 1 bar, and a temperature of 310 K, controlled with a Langevin baro- and thermostat, respectively. The simulations were run for a minimum of 50 ns, excluding the minimization, annealing and, equilibration steps (except for the second N501Y mutant ACE2-S1-RBD complex run which was run about 40 ns).

ACE2-S1-RBD molecular dynamics simulation trajectory analysis

Analysis of the trajectories was performed using the available tools in Visual Molecular Dynamics (VMD).[25] Independent root-mean-square deviation (RMSD) calculations for ACE2 and S1-RBD proteins was performed using the "RMSD trajectory Tool" in VMD.[25] Root-mean-square fluctuations (RMSF) measurements were performed using the indicated RMSF calculation script (Supporting Script 1). The distances between center of masses of specific pairs of amino acid residues such as Y41 and Y501 over the entire length of the simulation was determined using the indicated inter-residue center of mass distance calculation script (Supporting Script 2).

Timestep snapshot figures were prepared by saving trajectory coordinates in the PDB file format for each frame (500 frames, 10 frames/ns). The representative composite images shown in Figure 2 were prepared by combining a total 11 frames (every 5 ns). Representative trajectory movies of 50 ns simulations were prepares by compiling 100 trajectory snapshots (2 snapshots/ns) – that were generated utilizing VMD Movie Maker Tool [25] - using the Fiji image analysis software [26] with a frame-rate of 7/s to create 14 s movies.

Data Analysis and Figure Preparation

GraphPad Prism (version 9 for macOS, GraphPad Software, La Jolla California USA; www.graphpad.com), in combination with Microsoft Excel, was used for data analysis and graph preparation. Figures were assembled using Adobe Illustrator.

Results & Discussion

In order to understand the mechanism underlying increased affinity of the N501Y mutant over the wild type S1-RBD for ACE2, we initiated MD simulations with the available ACE2-S1-RBD complex structure (PDB ID: 6M0J)[21] (Fig. 1). We focused our attention on the N501 residue in S1-RBD and a closer inspection indicated that the residues Y41 and K353 in ACE2 are both located at the ACE2-S1-RBD interface and are in close proximity of N501 residue in S1-RBD (Fig. 1; outset). In fact, N501 has been shown to participate in hydrogen bonding (at 3.7 Å distance) with Y41 residue of ACE2, indicating its potential role in the ACE2-S1-RBD interaction.[21] For this, we initiated multiple, all-atom MD simulations in explicit solvent with the wilt type and the N501Y mutant ACE2-S1-RBD complex structure and analyzed the trajectories obtained for general structural dynamics and specific interactions. Further, we

155 performed the simulations in duplicates in order to test the consistency of the results and
156 statistical support.
157
158 Overall, these MD simulations revealed a generally decreased dynamics of the N501Y mutant
159 ACE2-S1-RBD complex compared to the wild type complex as seen from the composite image
160 of the complexes obtained from the simulation trajectories (Fig. 2A).[27-33] However, RMSD
161 analysis of the backbone Cα atoms of the proteins, ACE2 and S1-RBD individually taken over
162 the entire course of simulations time did not show any clearly discernable trend for structural
163 evolution of amino acid residues in the complex (Figure 2B,C). This suggests that any alteration
164 in the biochemical interaction between the two proteins likely arises due to changes in the
165 dynamics of specific, individual residues in the proteins. Indeed, RMSF analysis of individual
166 amino acid residues in the proteins showed a number of distinct changes with a general decrease
167 in the ACE2 in the N501Y mutant complex (Figure 2D). Specifically, residues positions at the
168 N-terminal (from 19 until 111), central (183 until 206) and to a smaller extent at the C-terminal
169 (from 542 until 588) of ACE2 showed a reduced RMSF values in the N501Y mutant complex.
170 Importantly, reduced RMSF values were observed for the Y41 and K353 residues in ACE2 in the
171 mutant complex. On the other hand, residues 281 to 283 in ACE2 showed an increased RMSF
172 value in the mutant complex.
173
174 RMSF analysis of S1-RBD showed a reduced structural fluctuation of Y501 in the mutant
175 complex compared to N501 in the wild type complex (Figure 2E), indicating an increased
176 interaction with adjacent, interfacial residues, likely in ACE2. Residue positions from 362 until
177 395 as well as the key 501 position of S1-RBD showed a substantially reduced RMSF values in

the mutant complex (Figure 2E). The latter is suggestive of the possibility of an allosteric effect of the increased interaction of Y501 in the mutant ACE2-S1-RBD complex as compared to N501 in the wild type complex.[27-33]

Following these analyses, we determined the residue-residue distances (based on the center of mass of the residues) of key residues at the ACE2-S1-RBD interface as they evolved during the span of the simulations (Figure 3A). First, N501 residue in the wild type complex showed a substantially higher structural fluctuation in comparison to Y501 in the mutant complex. In fact, as the simulation progressed, N501 in the wild type S1-RBD moved away from the ACE2-S1-RBD interface, with ACE2 Y41 residue moving in the other direction in the first simulation (Figure 3A; left panel). This was not the case for N501Y S1-RBD mutant, in which Y501 sustained its contact with at the ACE2-S1-RBD interface over the entire simulation time (Figure 3A; right panel). Indeed, the inter-residue distance analysis revealed a dramatic increase in the distance between Y41 and K353 in ACE2 and N501 in S1-RBD after about 30 ns in the simulation in the first simulation while a smaller increases at different times were seen in the second run (Figure 2B,C). This is in contrast to the distances measured for the same pair of ACE2 residues with Y501 in the mutant complex (~7 and 4.5 Angst, respectively) (Figure 2B,C). These data indicate the formation of a π-π stacking interaction between Y41 and Y501 and H-bond interaction between K353 and Y501 in the N501Y mutant complex.

In order to test if these effects of the N501Y mutation impacts interaction at the opposite end of the ACE2-S1-RBD interface, we monitored the inter-residue distances between the hydrogen bond forming Q24 in ACE2 and N487 in S1-RBD and closely juxtaposed (but not in hydrogen

bond) T27 in ACE2 and Y489 in S1-RBD [21]. In contrast to the observations made with the Y41-N501 and K353-N501 pairs, these pairs did not show any substantial fluctuations in their relative positioning (Figure 3D,E), suggesting that the effect of the N501Y mutation is largely local, and does not affect the overall interaction of ACE2 and S1-RBD in the timescales that we have explored here.

Conclusion

To conclude, the MD simulations performed here with the ACE2-S1-RBD complex provide an unambiguously mechanistic insight into the increased binding affinity of the N501Y mutant S1-RBD for ACE2. Specifically, our computational work shows that the mutation of N501 residue into a Y results in an increased and stable interaction with the Y41 and K353 residues in ACE2. This perhaps is positively impacted by the altered dynamics of the S1-RBD upon N501Y mutation, although the reason behind it is not entirely clear and will likely require further investigation. Although experiments determining binding of fluorescently labelled ACE2 and S1-RBD displayed on yeast cells and computational results presented here clearly indicate an increased affinity, it remains to be seen if the N501Y mutation alone can increase the overall fitness of the virus. The N501Y and associated mutations in the S1 spike protein has gained tremendous interest of the scientific community given that this lineage of SARS-CoV-2 has been suggested to be behind the dramatic increase in the number of COVID-19 cases in UK. We believe that the results outlined here will be helpful in efforts towards thwarting this new wave of COVID-19 by enabling discovery of potent inhibitors of ACE2-S1-RBD interaction [4-8].

Acknowledgements

This work is supported by an internal funding from the College of Health & Life Sciences, Hamad Bin Khalifa University, a member of the Qatar Foundation. W.A. and A.M.P. are supported by scholarship from the College of Health & Life Sciences, Hamad Bin Khalifa University, a member of the Qatar Foundation. Some of the computational research work reported in the manuscript were performed using high-performance computer resources and services provided by the Research Computing group in Texas A&M University at Qatar.

Research Computing is funded by the Qatar Foundation for Education, Science and Community Development (http://www.qf.org.qa).

Author Contributions

K.H.B. conceived the experiments. W.A, A.M.P. and K.H.B. performed experiments, analyzed data, prepared figures and wrote the manuscript. All authors reviewed and approved the manuscript.

Competing interests

The authors declare no competing interests.

Figures & Legends

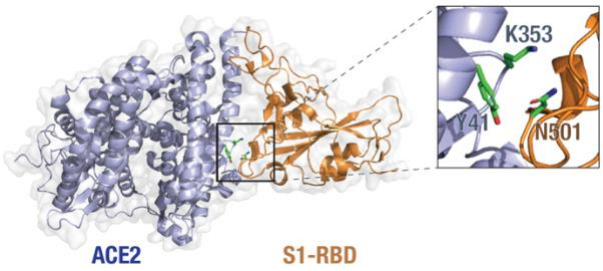

Figure 1. ACE2-S1-RBD interaction and the role of N501 residue. Cartoon representation of the ACE2-S1-RBD structure (PDB: 6M0J[21] showing the relative positioning of residues Y41 and K353 in ACE2 (light blue) and residue N501 in S1-RBD (orange).

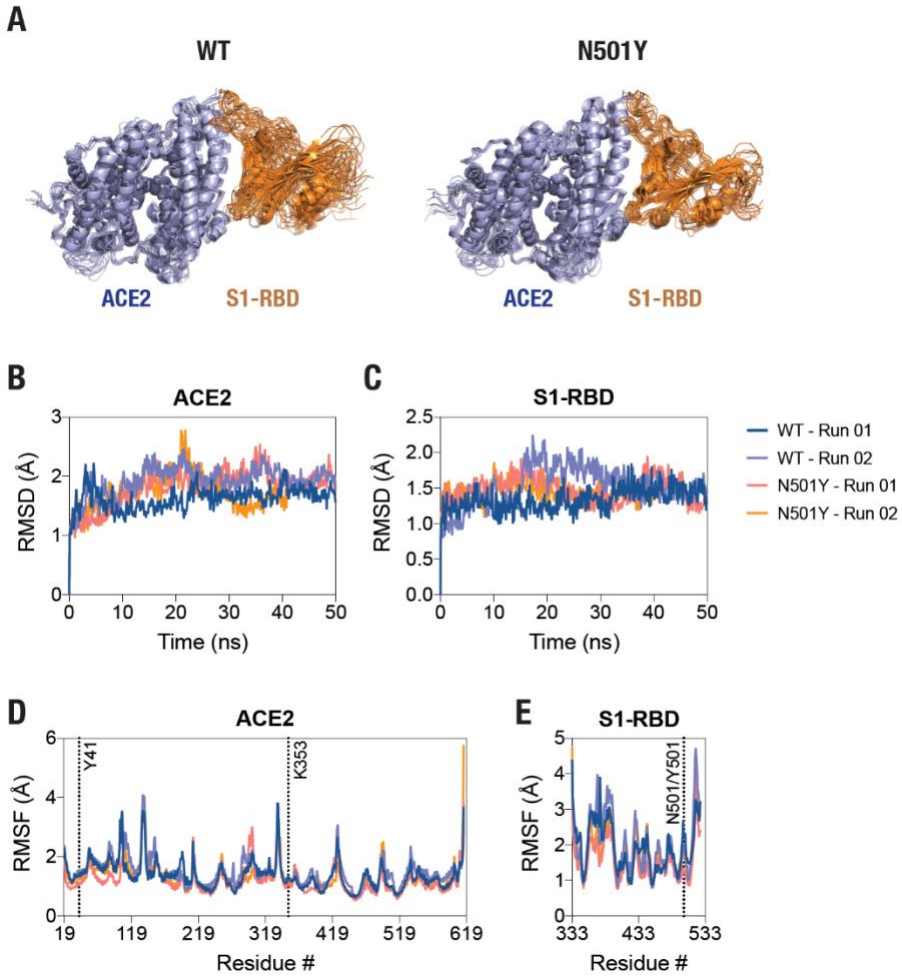

Figure 2. Decreased dynamics of the N501Y mutant S1-RBD in complex with ACE2. (A) Cartoon representation of the wild type (left panel) and the N501Y mutant (right panel) ACE2-S1-RBD complex showing structural evolution of the complex over time in a 50 ns all-atom, explicit solvent MD simulation. Composite images were prepared using 11 consecutive frames from up to 50 nm simulations with each frame 5 ns apart. (B,C) Graph showing backbone (Cα) root-mean-square deviation (RMSD) values of ACE2 (B) and S1-RBD (C) obtained from the simulation of the WT and N501Y mutant ACE2-S1-RBD complexes. (D,E) Graph showing backbone (Cα) root-mean-square fluctuation (RMSF) values of ACE2 (D) and S1-RBD (E) obtained from up to 50 nm simulations of the WT and N501Y mutant ACE2-S1-RBD complexes.

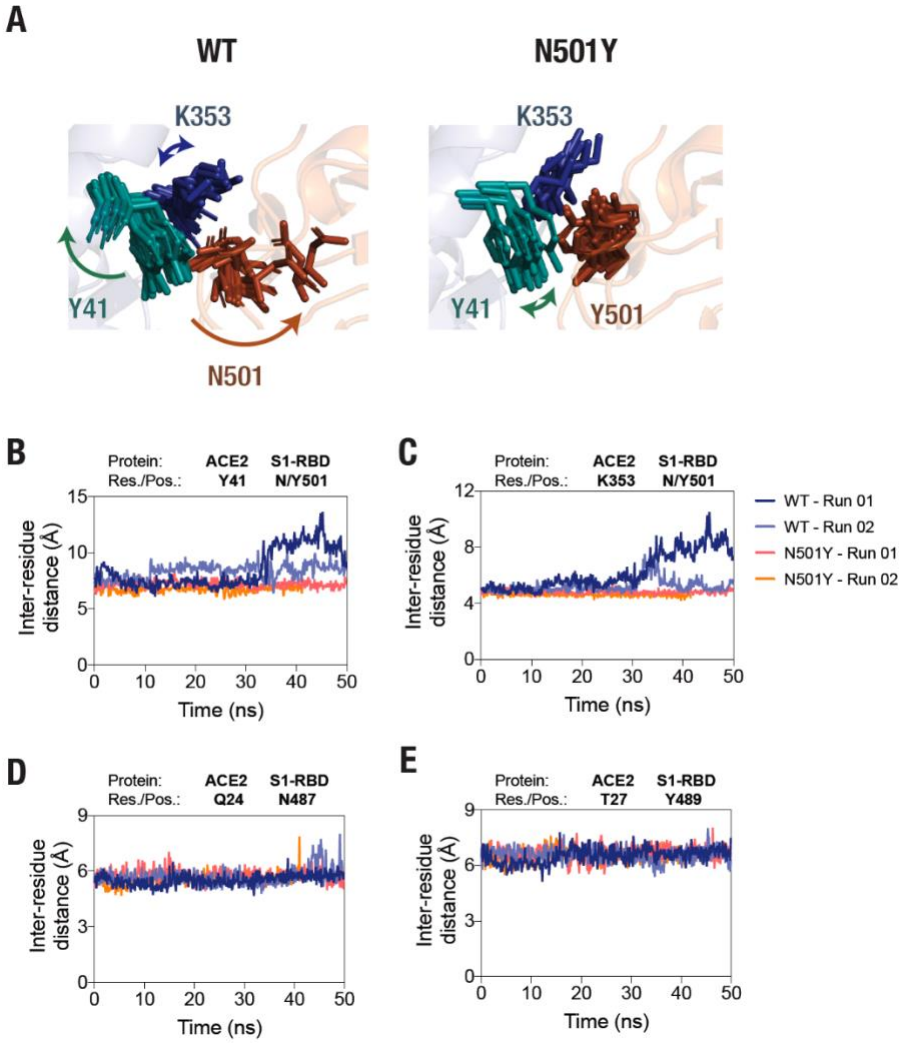

Figure 3. Sustained interaction of S1-RBD Y501 residue (N501Y mutant) with ACE2. (A) Temporal evolution of residues Y41 and K353 in ACE2 and either the N501 in the WT S1-RBD (left panel) or the Y501 in the N501Y mutant S1-RBD (right panel) in the MD simulation. A total of 11 frames obtained from up to 50 nm simulations, each 5 ns apart, were compiled together. Note the increased fluctuation of the N501 residue in the wild type S1-RBD. (B,C,D,E) Graph showing inter-residue distances (between center of masses) of residue Y41 in ACE2 and N501 in the wild type and Y501 in the N501Y mutant S1-RBD (B), K353 in ACE2 and N501 in the wild type and Y501 in the N501Y mutant S1-RBD (C), Q24 in ACE2 and N487 in either the

wild type or the N501Y mutant S1-RBD (D), and T27 in ACE2 and Y489 in either the wild type or the N501Y mutant S1-RBD (E). Note the increased inter-residue distance between the residues Y41 and K353 in ACE2 and N501 in S1-RBD in the wild type ACE2-S1-RBD complex (B,C) compared to the N501Y mutant complex.

References

1. Wu, F., et al., *A new coronavirus associated with human respiratory disease in China.* Nature, 2020. **579**(7798): p. 265.
2. V'Kovski, P., et al., *Coronavirus biology and replication: implications for SARS-CoV-2.* Nat Rev Microbiol, 2020.
3. Keidar, S., M. Kaplan, and A. Gamliel-Lazarovich, *ACE2 of the heart: From angiotensin I to angiotensin (1-7).* Cardiovascular research, 2007. **73**(3): p. 463.
4. Choudhary, S., Y. Malik, and S. Tomar, *Identification of SARS-CoV-2 Cell Entry Inhibitors by Drug Repurposing Using in Silico Structure-Based Virtual Screening Approach.* 2020.
5. Andersen, K.G., et al., *The proximal origin of SARS-CoV-2.* Nature Medicine, 2020: p. 1.
6. Shang, J., et al., *Structural basis of receptor recognition by SARS-CoV-2.* Nature, 2020.
7. Walls, A.C., et al., *Structure, Function, and Antigenicity of the SARS-CoV-2 Spike Glycoprotein.* Cell.
8. Wrapp, D., et al., *Cryo-EM structure of the 2019-nCoV spike in the prefusion conformation.* Science (New York, Ny), 2020. **367**(6483): p. 1260.
9. Zoufaly, A., et al., *Human recombinant soluble ACE2 in severe COVID-19.* Lancet Respir Med, 2020. **8**(11): p. 1154-1158.
10. Tai, W., et al., *Identification of SARS-CoV RBD-targeting monoclonal antibodies with cross-reactive or neutralizing activity against SARS-CoV-2.* Antiviral Res, 2020. **179**: p. 104820.
11. Avanzato, V.A., et al., *Case Study: Prolonged Infectious SARS-CoV-2 Shedding from an Asymptomatic Immunocompromised Individual with Cancer.* Cell, 2020. **183**(7): p. 1901-1912 e9.
12. Choi, B., et al., *Persistence and Evolution of SARS-CoV-2 in an Immunocompromised Host.* N Engl J Med, 2020. **383**(23): p. 2291-2293.
13. Plante, J.A., et al., *Spike mutation D614G alters SARS-CoV-2 fitness.* Nature, 2020.
14. Hou, Y.J., et al., *SARS-CoV-2 D614G variant exhibits efficient replication ex vivo and transmission in vivo.* Science, 2020. **370**(6523): p. 1464-1468.
15. Volz, E., et al., *Evaluating the Effects of SARS-CoV-2 Spike Mutation D614G on Transmissibility and Pathogenicity.* Cell, 2020.
16. Zhang, L., et al., *SARS-CoV-2 spike-protein D614G mutation increases virion spike density and infectivity.* Nat Commun, 2020. **11**(1): p. 6013.
17. Yurkovetskiy, L., et al., *Structural and Functional Analysis of the D614G SARS-CoV-2 Spike Protein Variant.* Cell, 2020. **183**(3): p. 739-751 e8.
18. Mansbach, R.A., et al., *The SARS-CoV-2 Spike Variant D614G Favors an Open Conformational State.* bioRxiv, 2020.
19. Andrew Rambaut, N.L., Oliver Pybus, Wendy Barclay, Jeff Barrett, Alesandro Carabelli, Tom Connor, Tom Peacock, David L Robertson, Erik Volz on behalf of COVID-19 Genomics Consortium UK (CoG-UK). *Preliminary genomic characterisation of an emergent SARS-CoV-2 lineage in the UK defined by a novel set of spike mutations*. 2020.

20. Santos, J.C. and G.A. Passos, *The high infectivity of SARS-CoV-2 B.1.1.7 is associated with increased interaction force between Spike-ACE2 caused by the viral N501Y mutation.* bioRxiv, 2021.
21. Lan, J., et al., *Structure of the SARS-CoV-2 spike receptor-binding domain bound to the ACE2 receptor.* Nature, 2020. **581**(7807): p. 215-220.
22. Starr, T.N., et al., *Deep Mutational Scanning of SARS-CoV-2 Receptor Binding Domain Reveals Constraints on Folding and ACE2 Binding.* Cell, 2020. **182**(5): p. 1295-1310. e20.
23. Phillips, J.C., et al., *Scalable Molecular Dynamics with NAMD.* Journal of computational chemistry, 2005. **26**(16): p. 1781.
24. Ribeiro, J.V., et al., *QwikMD - Integrative Molecular Dynamics Toolkit for Novices and Experts.* Sci Rep, 2016. **6**: p. 26536.
25. Humphrey, W., A. Dalke, and K. Schulten, *VMD: visual molecular dynamics.* Journal of molecular graphics, 1996. **14**(1): p. 33.
26. Schindelin, J., et al., *Fiji: an open-source platform for biological-image analysis.* Nature methods, 2012. **9**(7): p. 676-682.
27. Biswas, K.H., *Regulation of α-catenin conformation at cadherin adhesions.* J Biomech Sci Engg, 2018. **13**(4): p. 17-00699.
28. Biswas, K.H. and S.S. Visweswariah, *Buffer NaCl concentration regulates Renilla luciferase activity and ligand-induced conformational changes in the BRET-based PDE5 sensor.* Matters, 2017. **10.19185/matters.201702000015**.
29. Biswas, K.H., *Allosteric regulation of proteins.* Resonance, 2017. **22**(1): p. 37-50.
30. Biswas, K.H., et al., *Cyclic nucleotide binding and structural changes in the isolated GAF domain of Anabaena adenylyl cyclase, CyaB2.* PeerJ, 2015. **3**: p. e882.
31. Fiskerstrand, T., et al., *Familial diarrhea syndrome caused by an activating GUCY2C mutation.* N Engl J Med, 2012. **366**(17): p. 1586-95.
32. Biswas, K.H. and S.S. Visweswariah, *Distinct allostery induced in the cyclic GMP-binding, cyclic GMP-specific phosphodiesterase (PDE5) by cyclic GMP, sildenafil, and metal ions.* Journal of Biological Chemistry, 2011. **286**(10): p. 8545-54.
33. Biswas, K.H., S. Sopory, and S.S. Visweswariah, *The GAF domain of the cGMP-binding, cGMP-specific phosphodiesterase (PDE5) is a sensor and a sink for cGMP.* Biochemistry, 2008. **47**(11): p. 3534-43.

Supporting Information

Sustained Interaction Of The UK B.1.1.7 lineage SARS-CoV-2 S1 Spike N501Y Mutant With ACE2 Revealed By Molecular Dynamics Simulation

Wesam Ahmed[1], Angelin M Phillip[1], Kabir H Biswas[1,*]

Affiliation:

[1]College of Health & Life Sciences, Hamad Bin Khalifa University, Qatar Foundation, Doha – 34110, Qatar

***Correspondence:** kbiswas@hbku.edu.qa

Supporting Text

Script for calculating the RMSF value for residues in the protein-protein complex:

```
set reference [atomselect top "protein" frame 1]
# the frame being compared
set compare [atomselect top "protein"]
set num_steps [molinfo top get numframes]

for {set frame 0} {$frame < $num_steps} {incr frame} {
  # get the correct frame
  $compare frame $frame

  # compute the transformation
  set trans_mat [measure fit $compare $reference]
  # do the alignment
  $compare move $trans_mat
}


set outfile [open RMSF_script_output.txt w]
set sel [atomselect top "name CA"]
#puts $outfile "[measure rmsf $sel first 1 last 2000 step 1]"
set rmsf [measure rmsf $sel first 0 last 499 step 1]
for {set i 0} {$i < [$sel num]} {incr i} {
  puts $outfile "[expr {$i+1}] [lindex $rmsf $i]"
}
close $outfile
```

Script for calculating pair-wise inter-residue center-mass distance:

```
proc distance {seltext1 seltext2 N_d f_r_out f_d_out} {

     set sel1 [atomselect top "$seltext1"]
     set sel2 [atomselect top "$seltext2"]

     set nf [molinfo top get numframes]

     set outfile [open $f_r_out w]

     for {set i 0} {$i < $nf} {incr i} {
          puts "frame $i of $nf"
          $sel1 frame $i
          $sel2 frame $i
          set com1 [measure center $sel1 weight mass]
          set com2 [measure center $sel2 weight mass]
          set simdata($i.r) [veclength [vecsub $com1 $com2]]
          puts $outfile "$i , $simdata($i.r)"
     }

     close $outfile

     set r_min $simdata(0.r)
     set r_max $simdata(0.r)
     for {set i 0} {$i < $nf} {incr i} {
          set r_tmp $simdata($i.r)
          if {$r_tmp < $r_min} {set r_min $r_tmp}
          if {$r_tmp > $r_max} {set r_max $r_tmp}
     }

     set dr [expr ($r_max - $r_min) /($N_d - 1)]
     for {set k 0} {$k < $N_d} {incr k} {
          set distribution($k) 0
     }

     for {set i 0} {$i < $nf} {incr i} {
          set k [expr int(($simdata($i.r) - $r_min) / $dr)]
          incr distribution($k)
     }

     set outfile [open $f_d_out w]
     for {set k 0} {$k < $N_d} {incr k} {
          puts $outfile "[expr $r_min + $k*$dr] ,
$distribution($k)"
     }
     close $outfile
```

Supporting Movies

Supp. Movie 1. Trajectory movie displaying interaction between ACE2 and WT S1-RBD.

Movie was created by compiling 100 snapshots over 50ns simulation time (2 snapshots/1ns).

Movie frame-rate is 7/s.

Supplementary Movie 2. Trajectory movie displaying interaction between ACE2 and N501Y S1-RBD mutant. Movie was created by compiling 100 snapshots over 50ns simulation time (2 snapshots/1ns). Movie frame-rate is 7/s.